




Efficient SnO₂/CuO/porous silicon nanocomposites structure for NH₃ gas sensing by incorporating CuO nanoparticles

Husam R. Abed¹ · Alwan M. Alwan² · Ali A. Yousif¹ · Nadir F. Habubi¹ 

Received: 1 June 2019 / Accepted: 21 September 2019 / Published online: 30 September 2019
© Springer Science+Business Media, LLC, part of Springer Nature 2019

Abstract

In this paper, a porous silicon (Psi) surface modification process, including the incorporating of pure and CuO mixed SnO₂ within a Psi layer, was investigated. A Psi layer with a pore-like structure prepared via laser-assisted etching process with a laser illumination intensity of (40) mW/cm² was employed as a substrate for materialization SnO₂/CuO/Psi nanocomposites for gas sensing application. Pure SnO₂ and SnO₂:CuO nanoparticles were synthesized via a chemical spray pyrolysis process on the Psi surface at 350 °C. The materialization of SnO₂:CuO/Psi nanocomposites were recognized through Field-Emission Scanning Electron Microscopy, X-ray Diffraction, Atomic Force Microscopy, and Energy-dispersive X-ray Analysis. The results displayed that the morphological properties of SnO₂:CuO nanoparticles were definitely controlled by varying the CuO contents. Different shapes (nearly cubic shape and spherical shape) with various sizes of SnO₂ and SnO₂:CuO within the Psi surface were achieved by increasing the CuO content. SnO₂:CuO/Psi nanocomposites, plans, grain size, average surface roughness, homogeneity and specific surface area of SnO₂:CuO nanoparticles were considerably influenced by CuO content. The lower grain size and higher average surface roughness and specific surface area were attained when the percentage of CuO was about 30% within the structure of 70% SnO₂:30% CuO, and the performance of the NH₃ gas sensor revealed a short response time with a high sensitivity of (88%).

Keywords Nanocomposites · SnO₂:CuO · Spray pyrolysis · Porous silicon · NH₃

1 Introduction

Applications of Psi layer as a basic substrate for gas sensors process are of abundant significance as a global issue. The Psi surface modification process with a metal oxide semiconductor (MOS) ensures the extremely concerned attention owing to their stability and economic cost (An and Yang 2012; Kemmler et al. 2013; Huang and Wan 2009). Among the whole types of MOS, pure SnO₂ as a wide band gap of (3.5 eV) is broadly used in the

✉ Nadir F. Habubi
nadirfadhil@uomustansiriyah.edu.iq

¹ College of Education, Al - Mustansiriyah University, Baghdad, Iraq

² Department of Applied Sciences, University of Technology, Baghdad, Iraq

optoelectronics and solar cell applications (Dattoli et al. 2007; Chappel et al. 2002). On the other hand, the pure SnO₂ sensing element cannot provide the necessity for extreme detection for poisonous gases. So, a lot of alterations have been tried to enhance the gas sensing properties of SnO₂, like element incorporating (Zhang and Yang 2012), and combined with further metal oxide (Katoch et al. 2015). The more efficient process to enhance the physical and chemical properties and hence the gas sensing process is incorporating an alternative material to create a composite material (Paek et al. 2009; Huang et al. 2011; Kim et al. 2010). Several types of MOS, like In₂O₃, WO₃, ZnO, and CuO are incorporated to boost the gas sensing property. A unique favorable approach to improve the gas detection process is by growing the surface porosity while preserving the suitable sensing material at the surface, like using Psi substrates (Moshnikov et al. 2012). Many applications have been done on n-type PSi (Alwan and Dheyab 2017, Alwan et al. 2017, 2018; Ismail et al. 2016). One of the most important advantages of Psi layer is the simplistic preparation, inexpensive, low-temperature operation. The excellent specific surface area with well-regulated pore sizes makes the penetration of metal oxides into the silicon pores probable and also makes the Psi with metal oxide nanoparticles as a supreme convenient material for the preparation of MOS/Psi nanocomposites structure for the chemical gas sensors (Moshnikov et al. 2012; Bolotov et al. 2012; Naderi et al. 2012; Salonen et al. 2015). In the present work, a Psi surface modification process, including the incorporating of pure and CuO mixed SnO₂ nanoparticles within the Psi layer was investigated. An efficient SnO₂:CuO/Psi nanocomposites structure with excellent morphological properties is the main aim of this study, and hence to controlling and enhancing the gas sensing properties by improving the exposure area of nanocomposites/porous silicon structures through employing a specific form of SnO₂:CuO nanoparticles at specific positions within the porous layer.

2 Experimental work

2.1 Porous silicon formation

A Psi layer was prepared using mirror-like (100)-oriented n-type Si substrate with a resistivity of 10 Ω cm. Prior to the etching process; the SiO₂ was eliminated from the Si by rinsing the substrates in 10% HF aqueous solution for 5 min. The Psi layer was created via a laser-assisted etching process in an etching combination solution of 1:1 of 40% HF and 99.999% ethanol. The Si substrate was etched at a constant current density of around (18 mA/cm²) for 6 min with a laser wavelength of 650 nm and an intensity of 40 mW/cm² cm. Next to the etching process, the Psi substrate was washed with deionized pure H₂O and permitted to dry in the ambient atmosphere for a few minutes, Fig. 1 illustrates the experimental setup of the laser-assisted etching process.

2.2 Preparation of SnO₂:CuO/Psi nanocomposites structure

After the etching process, the Psi layer substrate is ready to deposit on by a spray pyrolysis process. As shown in Fig. 2, the experimental setup of the chemical spray pyrolysis process includes a solution that is sprayed on top of a Psi layer held at 350 °C, where the solution reacts to synthesize the preferred nanoparticle layer. The preliminary solution was achieved by aqueous solutions of 0.1 M SnCl₄·5H₂O from (BDH, ENGLAND) and 0.1 M CuCl₂ from (BDH, ENGLAND) and used as a doping agent to form multi mixing concentrations

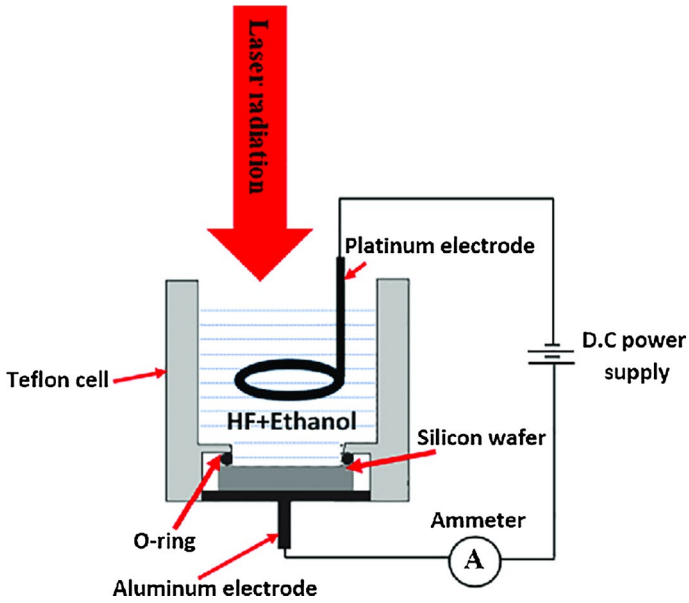


Fig. 1 Laser assisted etching setup

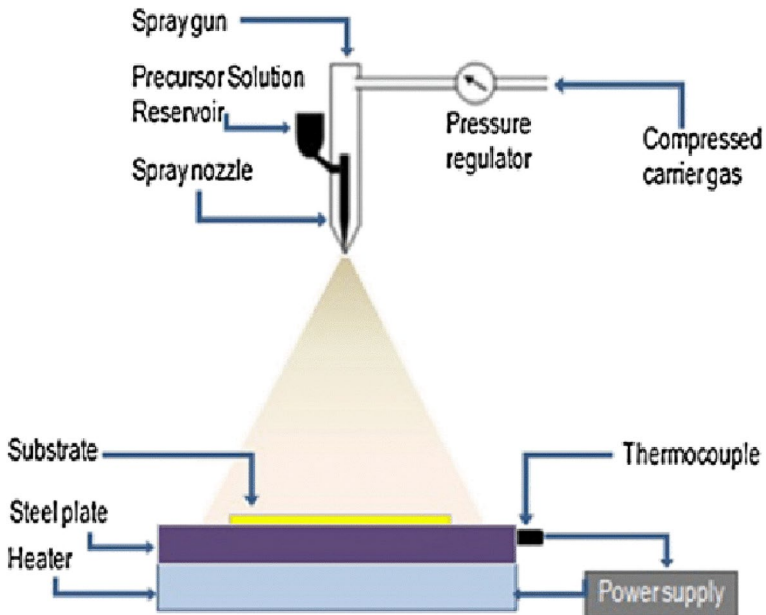


Fig. 2 Schematic diagram of spray pyrolysis experimental setup

(90%SnO₂:10%CuO, 70%SnO₂:30%CuO, 50%SnO₂:50%CuO). These compounds were melted in distilled deionized water, to form the required spray solution of 40 ml for every deposition route. The optimum conditions of the spraying procedure were found by using a glass atomizer, which has an output nozzle around 0.8 mm, for a spray time of 6 s, and the spray interval is about 60 s with a constant carrier nitrogen gas at a pressure of 3 bars, the distance between the nozzle and the Psi layer was about 15 cm with a flow rate of about 2.3 ml/min.

2.3 Characterization

The crystal structures of SnO₂ and SnO₂:CuO films were characterized by XRD diffractometer (Model-XRD- 6000 Shimadzu) using CuK α ($\lambda = 1.54056 \text{ \AA}$) radiation. Morphological properties of Psi surface before and after the modification process with pure and CuO mixed SnO₂ were investigated via using (FE-SEM) along with (EDXS) spectroscopy (INSPECT-550) and (CSP model AA3000 AFM supplied by Angstrom Company). The NH₃ sensing performances were made in a stationary gas performances characterization system comprising of a glass test cavity, a regular heating plate, and a programmable digital readout system. Aluminum ohmic contacts of 1 mm \times 0.5 mm were deposited by using thermal evaporation technique with a grid mask having a thickness of (300 nm) on the top of the SnO₂/CuO film surface. Sensing performances of Al/Psi/Al, Al/SnO₂/Psi/Al, and Al/SnO₂:CuO/Psi/Al device sensors have been successfully fabricated. The prepared sensors were investigated essentially in a vacuum case and with NH₃ gas of different concentrations 50 ppm, 100 ppm, and 150 ppm at the room temperature. The NH₃ was presented into the cavity straight to acquire the wanted concentration, and a programmable readout (UNI-UT70D) was employed for nonstop monitoring the current variation of the sensors by changing the voltage. The specimen interlude was set to 1 s, and the test temperature was the room temperature.

3 Results and discussion

3.1 X-ray diffraction patterns

The XRD patterns of the Psi layer, SnO₂, and SnO₂:CuO/Psi nanocomposites are elucidated in Fig. 3. Broader and definite XRD peaks were detected at 2 theta: 26.6, 33.9, 38.08 and 51.8 corresponding to (110), (101), (200) and (211) planes, respectively. This pattern is in a good agreement with the polycrystalline rutile structure of SnO₂ layer. Also, it is important to mention that the specific two peaks at around 2 theta: 33 and 38.9 are observed in the XRD pattern of SnO₂:CuO nanocomposite corresponding to (110) and (002) planes of CuO (Hwang et al. 2009), respectively. XRD patterns of SnO₂ and CuO displayed a good agreement with the diffraction data from JCPDS 41-1445 and 05-0661, correspondingly. From this pattern, it is clear that as the CuO content increases in SnO₂:CuO nanocomposite, the crystal size decreases, therefore, incorporating the CuO nanoparticles within the SnO₂ layer will improve the additional specific surface area over the Psi layer.

The crystallite size (*D*) was calculated using the Scherrer formula (Klug and Alexander 1974),

$$D = \frac{0.94\lambda}{L(2\theta) \cos \theta} \quad (1)$$

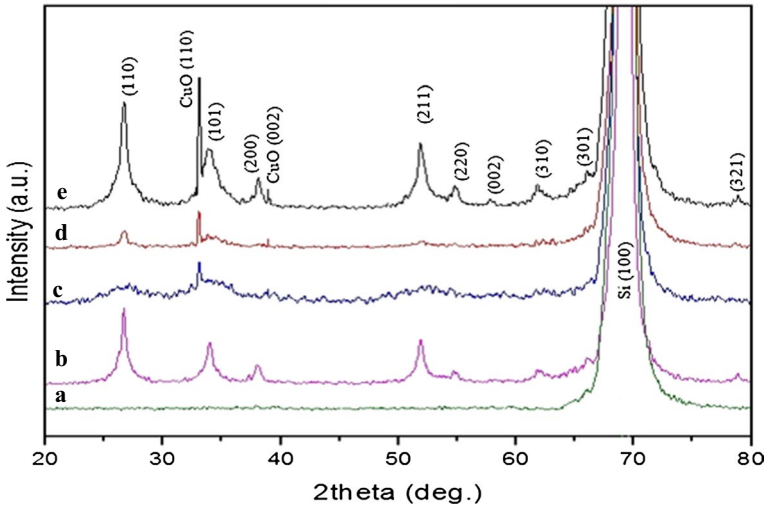


Fig. 3 XRD patterns of: (a) Bare Psi, (b) SnO₂, (c) 90%SnO₂:10%CuO, (d) 70%SnO₂:30%CuO and (e) 50%SnO₂:50%CuO

where λ is the wavelength of the X-ray of Cu K α radiation, and L is the full width at the half maximum of diffraction peaks. The values of crystal size were in the range from (25.1) to (13.3) nm for the unincorporated and the CuO incorporated SnO₂, correspondingly. Table 1 lists the crystal size and the specific surface area as a function of CuO content within SnO₂:CuO nanocomposite.

The specific surface area (S.S.A) of SnO₂:CuO nanocomposite is given by Hashim et al. (2018):

$$S.S.A = \frac{6000}{D \times \rho d} \quad (2)$$

where ρ is the density of SnO₂:CuO nanocomposite and it is calculated based on the density of SnO₂ and CuO by taking into account the percentage of elements in the EDS analysis (Hashim et al. 2018).

$$\rho_d = \frac{(a \times \rho)/(b \times \rho)}{a + b} \quad (3)$$

Table 1 Diffraction peaks, planes, crystallite size and the specific surface area within SnO₂:CuO nanocomposite

Sample	Main plane	2 θ	Crystal size (nm)	Specific surface area (m ² /gm)
Pure SnO ₂	110	26.66	25.1	34
90% SnO ₂ :10% CuO	110	26.73	18.3	47
70% SnO ₂ :30% CuO	110	26.7	13.5	63
50% SnO ₂ :50% CuO	110	26.69	15.4	56
90% SnO ₂ :10% CuO	110 (CuO)	33	17	55
70% SnO ₂ :30% CuO	110 (CuO)	33.05	13.3	71
50% SnO ₂ :50% CuO	110 (CuO)	33.02	14	67

where ρ is the density of the SnO₂ and CuO NPs, ρ_d is the density of SnO₂:CuO nanocomposite in g/cm³, $a = \text{wt\% SnO}_2$ and $b = \text{wt\% CuO}$ in the EDS analysis. The increase of S.S.A leads to enhance the interaction desorption and adsorption rates between the SnO₂-CuO layer and the gas molecules.

3.2 Morphological features of SnO₂:CuO/Psi Nanocomposites structures

The morphological nature of SnO₂ and SnO₂:CuO was investigated by analyzing the FESEM image, as shown in Fig. 4. The surface morphology of the Psi in Fig. 4a reveals that the structure is a pore-look like, rectangular and asymmetrical in shape due to the pores overlapping among the individual pores, and the pores are arbitrarily dispersed on the surface. This overlapping occurs due to the excessive etching process at a high laser illumination intensity (Alwan and Abdulrazaq 2008). The sizes of the pores are in the range of (0.8–2.7) μm , and the depth of the porous layer and the cross-sectional morphology of the deposited layer are evinced in the inset of each image. For pure SnO₂/Psi nanocomposites structure in Fig. 4b, the shapes of the pure SnO₂ nanoparticles deposited over the porous structure are nearly cubic with a size range of 80–95 nm. For the surface morphology of SnO₂:CuO/Psi nanocomposites at different CuO contents, Figs. 4c–e, it is clear that the SnO₂:CuO nanoparticles have a nearly spherical shape. Most of the nanoparticles are agglomerated at the silicon walls, and some of the nano sized CuO particles entered inside the pores of silicon, this is in a good agreement with (Ismail et al. 2016). With the increasing of CuO concentration from 10 to 50%, the resulting nanoparticles size decreases from 90 to 30 nm with improving the surface homogeneity, this reflects the important features for controlling the SnO₂:CuO nanoparticles and hence develops the extra specific surface over the native Psi layer. The nature of the sensing layer (SnO₂-CuO/Psi nanocomposites) is regulated by controlling the CuO content in the layer. This process is reflect a significant scientific touch for improving the sensing parameters.

The chemical structure of the SnO₂:CuO Nanocomposite was inspected by the EDS spectrum, as exposed in Fig. 5a–d. The elements Cu, Sn, O and Si are obvious, certainly confirming the existence of SnO₂:CuO nanocomposite. Also, from these figures, it can be noted that the peak of the specific elements was increased with increasing their contents in the synthesized SnO₂:CuO nanocomposite. The results of the element mapping for Sn, Cu and O are depicted in Fig. 5e–h. The spatial distributions of Sn, Cu, Si, and O clearly distinguish the CuO nanoparticles from SnO₂ ones.

3.3 AFM analysis

The topographical properties of Psi, SnO₂, and SnO₂: CuO nanocomposite are manifested in 2-D and 3-D AFM images in Fig. 6. The images clarify that the surface of all structures has a high degree of homogeneity without any cracks. The measured average surface roughness and the root mean square (RMS) obtained were increased with the increasing of CuO content, as shown in Table 2. In general, from this table, the roughness was increased with increasing CuO concentration, and a higher value of about (42.3 nm) was obtained at 30% CuO concentration. The increasing of the surface roughness will lead to enlarge the adsorption and the desorption rates between the NH₃ molecules and the active sensing elements. The granularity size spreading of the prepared particle sizes, as displayed in Fig. 6, specifies that the CuO content was definitely controlled by varying the surface properties of the deposited nanoparticles.

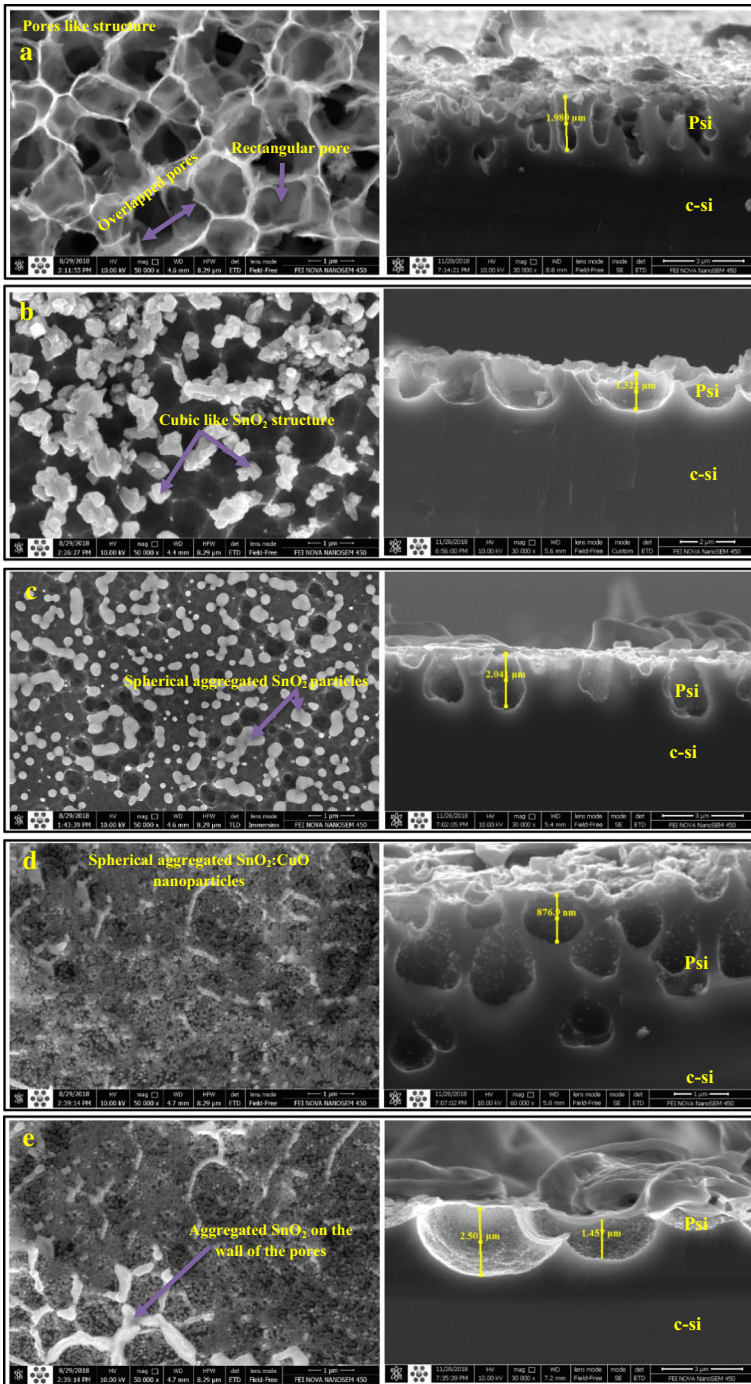


Fig. 4 FE-SEM images of: **a** Psi, **b** Pure SnO₂, **c** 90%SnO₂:10%CuO, **d** 70%SnO₂:30%CuO and **e** 50%SnO₂:50%CuO Nanocomposite. The inset images are cross section images

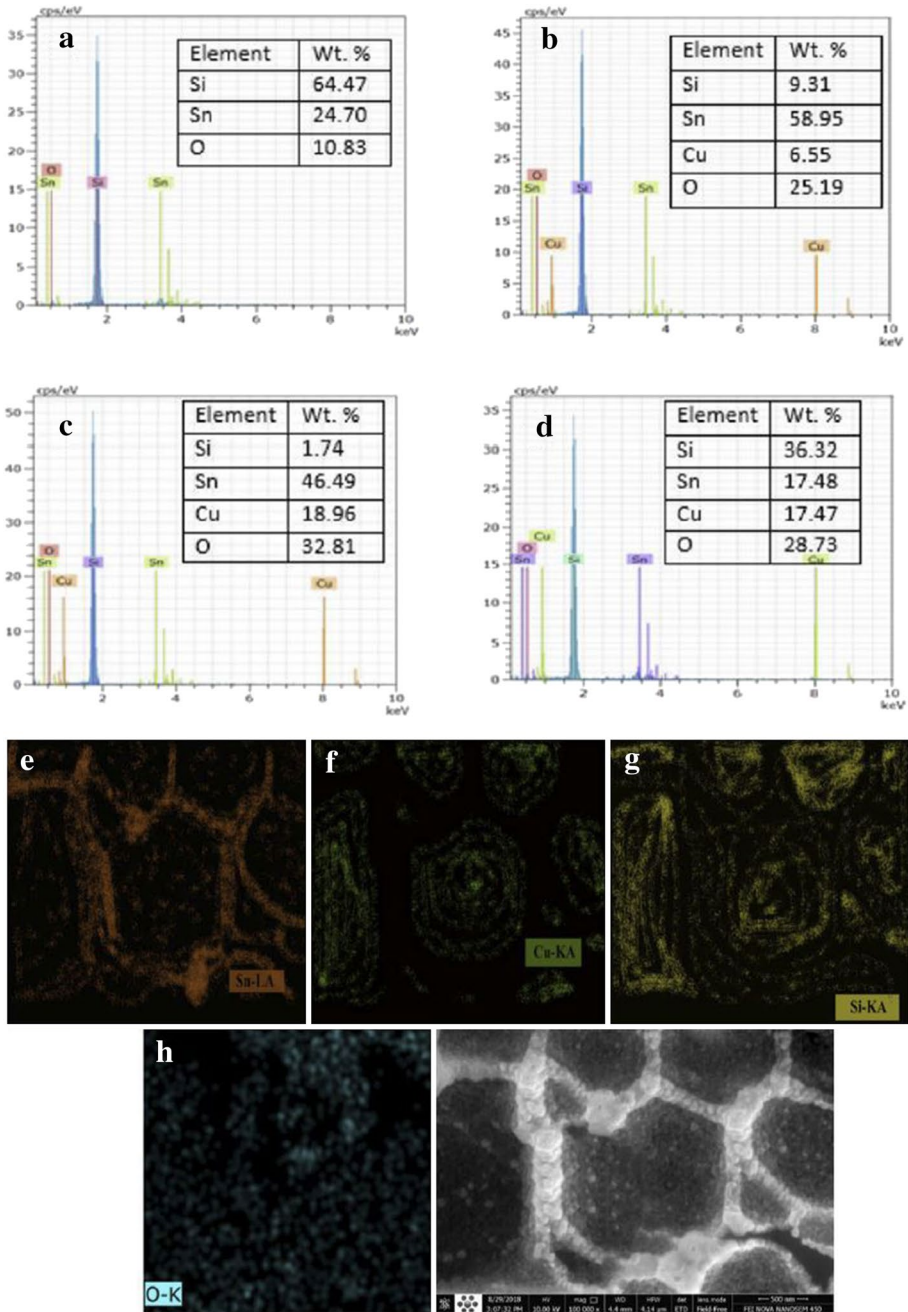


Fig. 5 EDS spectra: **a** Pure SnO₂, **b** 90%SnO₂:10%CuO, **c** 70%SnO₂:30%CuO, **d** 50%SnO₂:50%CuO and **e–h** Elemental mapping images of 70%SnO₂:30%CuO

Fig. 6 AFM image of: **a** PSi, **b** Pure SnO₂, **c** 90%SnO₂:10%CuO, **d** 70%SnO₂:30%CuO and **e** 50%SnO₂:50%CuO nanocomposite

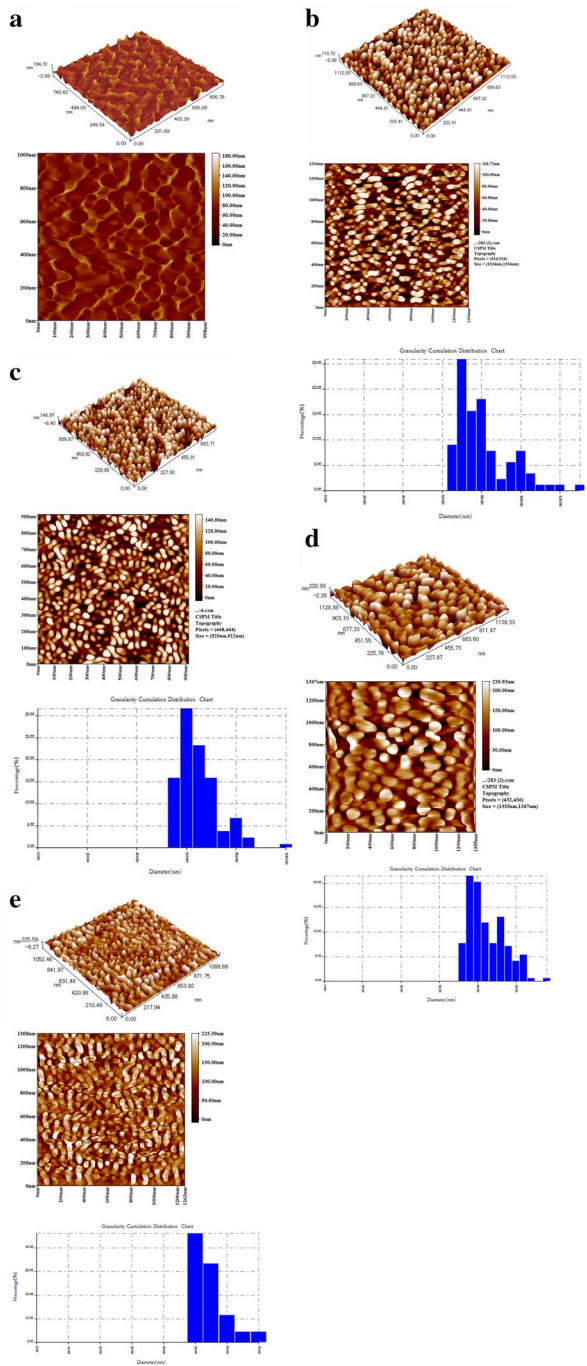


Table 2 Sample concentration, root mean square, roughness and average grain size obtained in the AFM analysis

Sample	Root mean square (nm)	Roughness (nm)	Average grain size (nm)
SnO ₂	35.6	30.7	78.33
90% SnO ₂ :10% CuO	44.7	38.8	62.3
70% SnO ₂ :30% CuO	51.6	42.3	41.5
50% SnO ₂ :50% CuO	47.7	39	51.94

3.4 Gas sensing characteristics

Al/PSi, Al/SnO₂, and Al/SnO₂:CuO sensors have been successfully fabricated, and the resistance as a function of time of NH₃ gas with different concentrations has been illustrated in Fig. 7. All sensors have been tested three times to confirm their gas performance. The Psi sensor showed a response and recovery times of values 15 s and 17 s, respectively. When the SnO₂ nanostructure was sprayed on the Psi, the response time enhanced by the value of 11 s, but with a long recovery time of 40 s. CuO nanoparticles have developed the sensor when 10% of them were loaded to 90% SnO₂ with a response and recovery times of 12 s and 14 s, respectively. The excellent sensor was obtained when 30% of CuO nanoparticles was incorporated into 70% SnO₂, this sensor elucidated a response and recovery times of 7 s and 20 s, respectively. The development in this sensor could be attributed to the small grain size and high specific surface area. The sensor 50% SnO₂:50% CuO evidenced a long response and recovery times. The decreasing of the response time (fast

Fig. 7 Resistance as a function of time of: (a) Al/PSi, (b) Al/SnO₂/PSi, (c) Al/90% SnO₂:10% CuO/PSi, (d) Al/70% SnO₂:30% CuO/PSi, and (e) Al/50% SnO₂:50% CuO/PSi

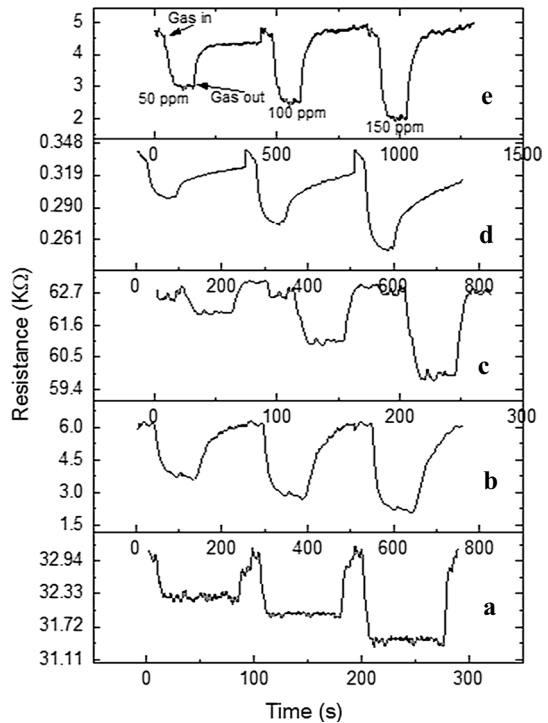
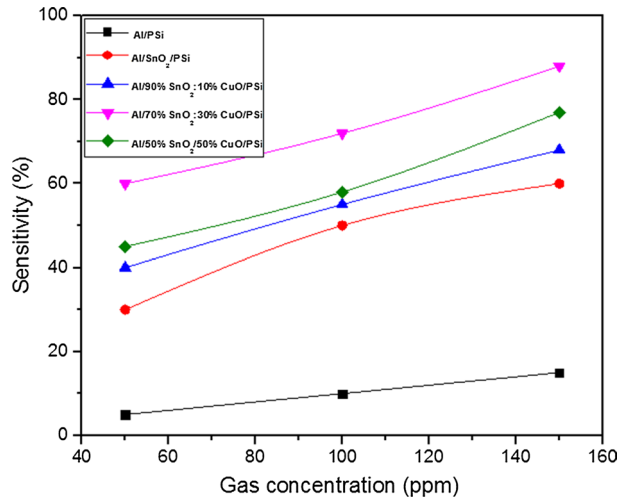


Fig. 8 Sensitivity as a function of NH₃ gas concentrations of Psi, SnO₂, and SnO₂:CuO nanocomposites sensors



sensing) of Psi with incorporating of SnO₂-CuO nanocomposites is due to the increasing of the adsorption rate between the sensing elements and the NH₃ molecules. Also the increasing of the recovery time is related to the desorption rate between the gas molecules and the active elements.

The sensitivity as a function of NH₃ gas concentrations is displayed in Fig. 8. Psi sensor showed the lowest sensitivity. This sensitivity improved when the SnO₂ nanostructure was deposited on the Psi layer with the value of (61%). As the 10% of CuO nanoparticles was modified to 90% SnO₂, the sensitivity increased to (68%). The best value of sensitivity was observed when 30% of CuO was added to 70% SnO₂ and it recorded (88%), this value is better than that reported in Yan et al. (2019), Ganesh et al. (2018) and Jahromi and Behzad (2018). The sensitivity was calculated by Alwan et al. (2019):

$$\text{Sensitivity} = \frac{R_g}{R_a} \quad (4)$$

where, R_g is the resistance measured in the presence of the target gas, and R_a is the resistance measured in the presence of air.

4 Conclusions

In this work, efficient MOS/Psi nanocomposites structure was successfully synthesized by incorporating pure SnO₂ and CuO mixed with SnO₂ nanoparticles into a Psi layer. Controlling the CuO content changes efficiently the morphology of the Psi surface. A high degree of homogeneity with a high average surface roughness, high root means square (RMS) and highly extra specific surface over the native Psi layer were achieved by 30% CuO content layer. The gas sensor properties evidenced a short response and recovery times with a very high sensitivity. Further works in the application of these new MOS/Psi nanocomposites will expose a unique prospect in the field of applied Nanosciences.

Acknowledgements The authors would like to thank University of Technology, Baghdad-Iraq, Mustansiriyah University, Baghdad-Iraq, and University of Tehran, Tehran-Iran, for their support in the present work.

References

- Alwan, A.M., Abdulrazaq, O.A.: Aging effect on the photosynthesized porous silicon. *Int. J. Mod. Phys. B* **22**, 417–422 (2008)
- Alwan, A.M., Dheyab, A.B.: Room temperature CO₂ gas sensors of AuNPs/mesoPSi hybrid structures. *J. Appl. Nanosci.* **7**, 335–341 (2017)
- Alwan, A.M., Yousif, A.A., Wali, L.A.: A study on the morphology of the silver nanoparticles deposited on the n-type porous silicon prepared under different illumination types. *Plasmonics* **13**, 1191–1199 (2017)
- Alwan, A.M., Abbas, R.A., Dheyab, A.B.: Study the characteristic of planar and sandwich PSi gas sensor (comparative study). *J. Silicon* **10**, 2527–2534 (2018)
- Alwan, A.M., Hashim, D.A., Jawad, M.F.: Efficient bimetallic nanoparticles embedded-porous silicon CO gas sensor. *Solid State Electron.* **153**, 37–45 (2019)
- An, W., Yang, C.: Progress of research on preparation of micro gas sensors of metal oxide semiconductors. *Appl. Mech. Mater.* **143–144**, 562–566 (2012)
- Bolotov, V.V., Korusenko, P.M., Nesov, S.N., Povoroznyuk, S.N., Roslikov, V.E., Kurdyukova, E.A., Sten'kin, Y.A., Shelyagin, R.V., Knyazev, E.V., Kan, V.E., Ponomareva, I.V.: Nanocomposite por-Si/SnOx layers formation for gas microsensors. *Mater. Sci. Eng. B* **177**, 1–7 (2012)
- Chappel, S., Chen, S.-G., Zaban, A.: TiO₂-coated nanoporous SnO₂ electrodes for dye-sensitized solar cells. *Langmuir* **18**, 3336–3342 (2002)
- Dattoli, E.N., Wan, Q., Guo, W., Chen, Y., Pan, X., Lu, W.: Fully transparent thin film transistor devices based on SnO₂ nanowires. *Nano Lett.* **7**, 2463–2469 (2007)
- Ganesh, R.S., Durgadevi, E., Navaneethan, M., Patil, V.L., Ponnusamy, S., Muthamizhchelvan, C., Kawasaki, S., Patil, P.S., Hayakawa, Y.: Tuning the selectivity of NH₃ gas sensing response using Cu-doped ZnO nanostructures. *Sens. Actuators A Phys.* **269**, 331–341 (2018)
- Hashim, D.A., Alwan, A.M., Jawad, M.F.: An investigation of structural properties of monometallic (Ag, Pd) and bimetallic (Ag@Pd) nanoparticles growth on macro porous silicon. *Int. J. Nanoelectron. Mater.* **11**, 461–472 (2018)
- Huang, J., Wan, Q.: Gas sensors based on semiconducting metal oxide one-dimensional nanostructures. *Sensors* **9**, 9903–9924 (2009)
- Huang, X.D., Zhou, X.F., Zhou, L., Qian, K., Wang, Y.H., Liu, Z.P.: A facile one-step solvo thermal synthesis of SnO₂/graphene nanocomposite and its application as an anode material for lithium-ion batteries. *ChemPhysChem* **12**, 278–281 (2011)
- Hwang, I.S., Choi, J.K., Kim, S.J., Dong, K.Y., Kwon, J.H., Ju, B.K., Lee, J.H.: Enhanced H₂S sensing characteristics of SnO₂ nanowires functionalized with CuO. *Sens. Actuators B* **142**, 105–110 (2009)
- Ismail, R.A., Alwan, A.M., Ahmed, A.S.: Preparation and characteristics study of nano-porous silicon UV photodetector. *Appl. Nanosci.* **7**, 9–15 (2016)
- Jahromi, H.S., Behzad, M.: Construction of 0, 1, 2 and 3 dimensional SnO₂ nanostructures decorated by NiO nanopetals: structures, growth and gas-sensing properties. *Mater. Chem. Phys.* **207**, 489–498 (2018)
- Katoch, A., Kim, J.-H., Kwon, Y.J., Kim, H.W., Kim, S.S.: Bi functional sensing mechanism of SnO₂-ZnO composite nanofibers for drastically enhancing the sensing behavior in H₂ gas. *ACS Appl. Mater. Interfaces* **7**, 11351–11358 (2015)
- Kemmler, J.A., Pokhrel, S., Maedler, L., Weimar, U., Barsan, N.: Flame spray pyrolysis for sensing at the nanoscale. *Nanotechnology* **24**, 442001–442014 (2013)
- Kim, H., Kim, S.W., Park, Y.U., Gwon, H., Seo, D.H., Kim, Y.: SnO₂/grapheme composite with high lithium storage capability for lithium rechargeable batteries. *Nano Res.* **3**, 813–821 (2010)
- Klug, H.P., Alexander, L.E.: *X-Ray Diffraction Procedures for Polycrystalline and Amorphous Materials*, 2nd edn. Wiley, New York (1974)
- Moshnikov, V.A., Gracheva, I., Lenshin, A.S., Spivak, Y.M., Anchkov, M.G., Kuznetsov, V.V., Olchowik, J.M.: Porous silicon with embedded metal oxides for gas sensing applications. *J. Non Cryst. Solids* **358**, 590–595 (2012)
- Naderi, N., Hashim, M.R., Amran, T.S.T.: Enhanced physical properties of porous silicon for improved hydrogen gas sensing. *Superlattices Microstruct.* **51**, 626–634 (2012)
- Paek, S.M., Yoo, E., Honma, I.: Enhanced cyclic performance and lithium storage capacity of SnO₂-graphene nanoporous electrodes with three-dimensionally delaminated flexible structure. *Nano Lett.* **9**, 72–75 (2009)
- Salonen, J., Kaasalainen, M., Rauhala, O.-P., Lassila, L., Hakamies, M., Jalkanen, T., Hahn, R., Schmuki, P., Makila, E.: (Invited) thermal carbonization of porous silicon: the current status and recent applications. *ECS Trans.* **69**, 167–176 (2015)

- Yan, F., Shen, G., Yang, X., Qi, T., Sun, J., Li, X., Zhang, M.: Low operating temperature and highly selective NH₃ chemiresistive gas sensors based on Ag₃PO₄ semiconductor. *Appl. Surf. Sci.* **479**, 1141–1147 (2019)
- Zhang, X., Yang, H.: Structural characterization and gas sensing property of Cd-doped SnO₂ nanocrystallites synthesized by mechanochemical reaction. *Sens. Actuators B* **173**, 127–132 (2012)

Publisher's Note Springer Nature remains neutral with regard to jurisdictional claims in published maps and institutional affiliations.